Brain–Computer Interface for Fuzzy Position Control of a Robot Arm by Mentally Detected Magnitude and Sign of Positional Error

Arnab Rakshit and Amit Konar

Abstract The paper addresses a novel approach to position control of a robot arm by utilizing three important brain signals, acquired with the help of an EEG interface. First, motor imagery signal is employed to activate the motion of a robotic link. Second, the error-related potential signal is acquired from the brain to stop the motion of the robotic link, when it crosses a predefined target position. Third, the approximate magnitude of the positional error is determined by steady-state visual evoked potential signal, acquired by noting the nearest flickering lamp that the robotic link has just crossed. The novelty of the present research is to decode the approximate magnitude of the positional error. Once the approximate magnitude and sign of the positional errors are obtained from the mental assessment of the experimental subject, the above two parameters are fed to a fuzzy position controller to generate necessary control commands to control the position of the end-effector of the robotic link around the predefined target position. Experiments undertaken confirm a low percentage of overshoot and small settling time of the proposed controller in comparison to those published in the current literature.

Keywords EEG · Robotic arm · ERD/ERS · ErrP · SSVEP · Fuzzy control

1 Introduction

Brain–computer interface (BCI) is currently gaining increasing potential for its widespread applications in rehabilitative robotics. People with neuro-motor disability such as Amyotrophic Lateral Sclerosis (ALS), partial paralysis, and the like require assistive support to perform their regular day-to-day works, such as delivery of food

A. Rakshit (✉) · A. Konar
Department of Electronics & Tele-communication Engineering, Jadavpur University, Kolkata, India
e-mail: arnabrakshit2008@gmail.com

A. Konar
e-mail: konaramit@yahoo.co.in

S. Bhattacharyya et al. (eds.), *Intelligent Systems and Human Machine Collaboration*,
Lecture Notes in Electrical Engineering 985,
https://doi.org/10.1007/978-981-19-8477-8_13

[1], medicines [2], etc. by an artificial robotic device, where the patients themselves can control the movements of the robot arm, their pick-up, placements, etc. by mind-generated control commands. Neuro-prosthesis is one of the most active areas of BCI research for its inherent advantage to rehabilitate people with degenerative neuro-motor diseases. Early research on neuro-prosthetics began with the pioneering contribution of Pfurtscheller [3, 4], who experimentally could first demonstrate the scope of one fundamental brain signal, called Motor Imagery, technically titled as Event-Related Desynchronization followed by Event-Related Synchronization (ERD/ERS). This signal appears in the motor cortex region of a person, when he/she thinks of moving his/her arms/legs or any voluntarily movable organs. Several researchers have utilized this signal for mind-driven motion-setting to a mobile robot [5], local navigating device [6, 7], artificial robotic arm [8–10], and many others. However, using ERD/ERS signal alone can switch on or switch off a device, and thus can only be used for open-loop applications.

In order to utilize the ERD/ERS in closed-loop position control applications, we need additional brain signals. Several research groups [11–13] have taken initiatives to utilize the benefits of Error-Related Potential (ErrP) and/or P300 signals to develop a generic platform for closed-loop position control applications. It is important to mention here that the ErrP signal is liberated from the z-electrodes, located at the midline of our scalp, when a subject himself commits any motion-related error and/or finds a second person or a machine to commit similar errors. The ERD/ERS and ErrP signals have been employed in a number of robot position control systems to set in motion of the robotic motor on emergence of the MI (ERD/ERS signal) and switch off the motor of the robot arm, when the robotic link crosses a fixed target position. However, the primary limitation of such position control schemes is on–off control strategy, which according to classical control theory results in large steady-state error [14].

To overcome this problem, several extensions to the basic control strategies have been proposed in the recent past [13, 15]. In [15], the authors developed a new strategy to reduce large steady-state error by commanding the robot to turn in reverse direction at a relatively lower speed than its current speed and also sensing the second, third P300, when the target is crossed several times by the end-effector. Such scheme can result in reduced steady-state error but at the cost of extra settling time.

The present research can reduce both steady-state error and settling time as it happens to be in case of classical control strategy by assessing the sign and magnitude of positional error from the subject's brain. However, as the magnitude of error is approximate, a fuzzy controller is a more appropriate option in contrast to a traditional controller. A set of fuzzy rules are proposed to infer the position of the end-effector from the approximate magnitude and sign of positional errors. Traditional Mamdani-type fuzzy reasoning is employed to yield the fuzzified end-effector positions. In case a number of fuzzy rules fire synchronously, the union of the inferences is considered. Finally, a defuzzifier is used to get back the controlled position of the end-effector. The proposed approach thus is unique and remained unknown to the BCI research community.

The paper is divided into five sections. In Sect. 2, we provide the principles adopted for position control using magnitude and sign of error, captured from the acquired ErrP and SSVEP signals. Section 3 deals with a discussion on processing of the acquired brain signals to make them free from noise and extraction of certain features from the pre-processed signals for classification. Section 4 deals with fuzzy controller design. Section 5 covers the experimental issues and also narrates the main results justifying the claims. A list of conclusions is included in Sect. 6.

2 Principles Adopted in the Proposed Position Control Scheme

This section provides the principles of position control using three brain signals: (i) motor imagery to actuate the motion of a robotic link, (ii) stopping the robotic link by sensing the ErrP signal, and (iii) assessing the magnitude of positional error from the flickering Light Emitting Diode (LED) closest to the stopping position. It is indeed important to mention here that assessment of the magnitude of error by SSVEP introduced here is novel and primary contribution of the present research. The sign and the magnitude of positional error together help in generating the accurate control action for the position control application. The principles of the BCI-based position control scheme are given in Fig. 1. It is noteworthy from Fig. 1 that the controller receives both sign and magnitude of error to generate the control signal. However, the exact measure of the magnitude of error cannot be performed easily for practical limitation in placement of SSVEP sources continuously along the trajectory of motion of the robotic end-effector. To overcome the present problem, an approximate assessment of the positional error is evaluated in five scales: NEAR ZERO, SMALL POSITIVE, LARGE POSITIVE, SMALL NEGATIVE and LARGE NEGATIVE using fuzzy membership functions [16]. The control signal about position of the end-effector is also fuzzified in the same five scales. Such assessment helps in generating fuzzy inferences about the degree of memberships of control signals in multiple fuzzy sets. It is indeed important to mention here that a fuzzy system usually is much robust in comparison to traditional rule-based expert systems as it takes care of aggregation of the inferences obtained from firing of multiple rules simultaneously by taking fuzzy union of the generated inferences. The defuzzification of the overall inference returns the signal back in the real domain. There exist several defuzzification procedures. Here, the center of gravity (CoG) defuzzification is used for its simplicity and wide popularity in fuzzy research community [17].

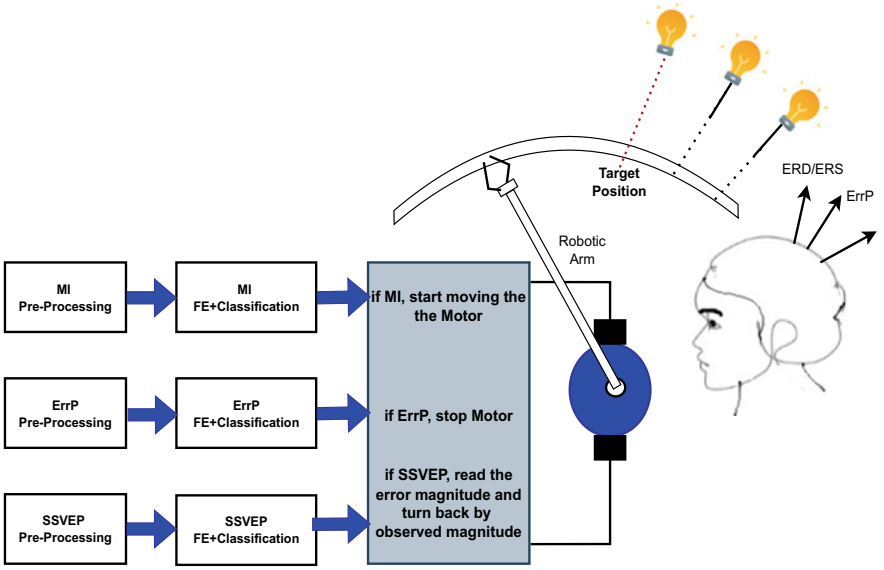

Fig. 1 Overview of BCI-based position control scheme

3 Signal Processing and Classification of Brain Signals

This section provides an overview of the basic signal processing, feature extraction, and classifier design aspects for the proposed application.

3.1 ERD-ERS Feature Extraction and Classification

For ERD-ERS feature extraction, we need to take as many as 500 offline instances of motor imagery (MI) signals acquired from the motor cortex regions of the subject. These 500 instances of MI signals are examined manually to identify around 300 true positive (v-shaped) and around 200 false negative (non-V or V with inadequate depth) instances. Both the true positive and false negative instances are then sampled at a fixed interval of time, and the mean and variance of the signals at each sampled point are evaluated. Let, at a given sample point s_i, we obtain 300 values from 300 true positive curves. Now a Gaussian model is constructed for each sample point s_i, with mean $= m_i$ and standard deviation σ_i. The sample values that lie within $m_i \pm 3\sigma_i$ are used and the rest are discarded. Thus, for each time position in the training samples, we accommodate selected values of the existing trials. Similarly, we undertake selective sample values from a pool of 200 EEG false negative instances. These true positive and false negative instances of the ERD/ERS signals are used subsequently to train a classifier. In this paper, Common Spatial Pattern (CSP), which

is widely used in BCI literature as an optimized spatial filter [18], is employed to evaluate the data covariance matrices for the two classes to effectively project the training samples into CSP features. These CSP features are then transferred to a two-level classifier to recognize the positive and negative motor imagery (MI) signals.

For classification of MI and resting conditions (also called NO motor imageries), the following steps are followed. Let X_1 and X_2 be $m \times n$ matrices, where m and n, respectively, denote number of EEG channels and number of time samples. Let $C1$ and $C2$ be the spatial covariance matrices given by $C1 = X_1 X_1^T$ and $C2 = X_2 X_2^T$ for positive (MI) and false negative classes. The motivation of CSP is to obtain filter vector $\mathbf{w}$, such that the scalar $\mathbf{wC_1w^T/wC_2w^T}$ is maximized. Once optimal value of vector w is evaluated, the variances of CSP projections $\mathbf{wX_1}$ and $\mathbf{wX_2}$ are utilized as CSP features of two classes. Any traditional linear classifier, such as Linear Discriminant Analysis (LDA) or Linear Support Vector Machine (LSVM), and the like can be used for classification of the MI signals from the resting states. Here, the authors employed Kernelized Support Vector Machine (KSVM) with Radial Basis Function (RBF) kernel for its proven accuracy in high-dimensional non-linear classification [19].

3.2 ErrP Feature Extraction and Classification

Previous research on ErrP feature extraction reveals that the characteristics of ErrP signal can be better captured by time-domain parameters, such as Adaptive Autoregressive (AAR) coefficients [13]. This inspired the authors to utilize AAR features for the detection of ErrP. In the present research, AAR parameters are extracted from approximately 500 ErrP instances and 500 resting states in offline training phase. A q-order AAR expresses each EEG sample as a linear combination of past q samples along with an error term characterized by zero mean Gaussian process. AAR coefficients are estimated using Least Mean Square (LMS) algorithm with an update parameter of 0.0006. For an EEG signal of 1s duration (200 samples), a 6th-order AAR generates $6 \times 200 = 1200$ AAR parameters which are used as the feature vector of the EEG trial. An LSVM classifier is then developed to determine the unique set of weights of the classifier to classify the ErrP and non-ErrP instances in real time.

3.3 SSVEP Detection

For detection of SSVEP, the occurrence of the peak power at the flickering frequency of the stimulus is checked. To test this, the maximum power in the PSD is searched over the frequency spectrum. If there is a single peak power occurring at the flickering frequency, then SSVEP is confirmed. In this study, we estimated the spectral power density through Welch's modified periodogram method [20]. Power spectral density

is obtained for each stimulus frequency and their first two harmonics. We considered an interval 1 Hz below and above the stimulus frequency to obtain the PSD. Once the PSD values associated to each SSVEP stimulus frequency are obtained, we search for the frequency that has highest PSD value. The frequency having the highest frequency value is considered as the target stimulus.

4 Fuzzy Controller Design

The novelty of the current paper is to determine the controller response from the approximate measure of magnitude of error. Here, the occurrence of the error signal is determined from the occurrence of ErrP signal. Now, to measure the magnitude of the error signal, a set of flickering light sources are placed at regular intervals. All these sources flicker at disjoint frequencies. When the subject observes the robotic arm crossing the target position, he is supposed to yield an ErrP signal from the z-electrodes. Almost simultaneously, he is supposed to release an SSVEP signal. Generally, people suffering from neuro-motor diseases have relatively poor reflex, and so they take longer time to respond to flickering visual signals. In order to alleviate this problem, light sources flickering at different frequencies are placed around their trajectory of the end-effector. Here, the subject has to pay attention to the nearest flickering source, close enough to the terminal position of the end-effector. Here, the flickering signal of the sources has frequencies in the ascending order of their distances from the predefined target position. This makes sense in the way that larger is the distance of the flickering source from the target position, the larger is the frequency of the source. A set of fuzzy quantifiers is employed to quantify the measure of the positional error in five grades: NEAR ZERO(NZ), SMALL POSITIVE(SP), LARGE POSITIVE(LP), SMALL NEGATIVE(SN) and LARGE NEGATIVE(LN). A knowledge base comprising a set of rules that map the fuzzified errors into fuzzy control signals is then utilized to derive the control signals for each fired rule. The union of the fuzzy control signals is taken, and the result is defuzzified to get back the actual value of the control signal.

4.1 Fuzzy Reasoning in the Control Problem

Consider the fuzzy production rules:

Rule 1: If x is A_1 then y is B_1
Rule 2: If x is A_2 then y is B_2
$\vdots$
Rule n: If x is A_n then y is B_n

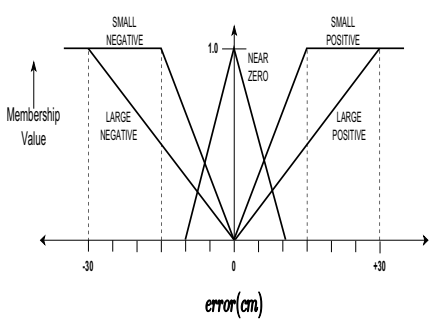

(a) Membership function: error

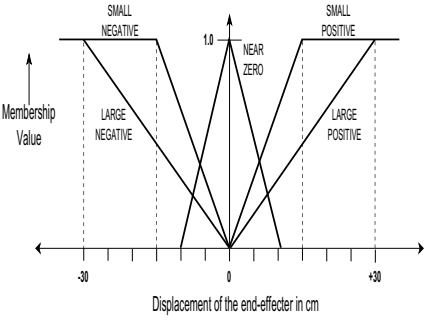

(b) Membership function: angular displacement

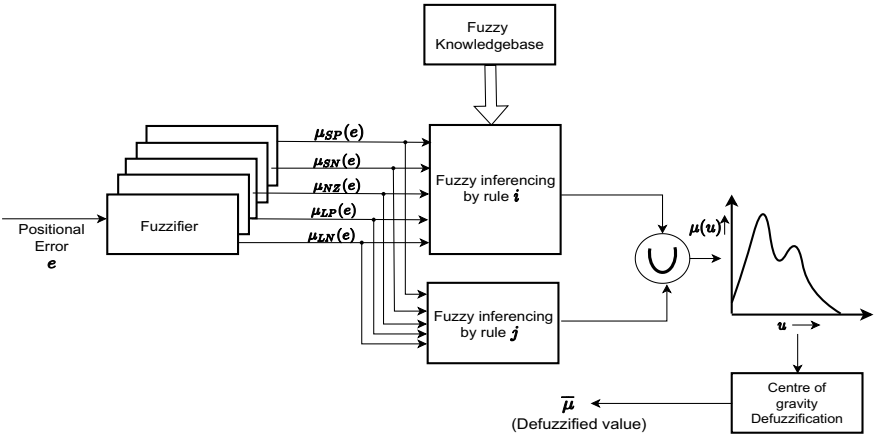

(c) Architecture of the proposed fuzzy controller

Fig. 2 Architecture of the proposed fuzzy controller and schematic overview of membership curves

Here x,y are linguistic variables in the universes X and Y, respectively. $A_1, A_2, \ldots, A_n$ are fuzzy sets under the universe X and $B_1, B_2, \ldots, B_n$ are fuzzy sets under the universe Y. Let $x = x'$ be a measurement. We compute the fuzzy inference for the given measurement $x = x'$ by the following steps:

Step 1: Compute: $\alpha_1 = Min(\mu_{A_1}(x'), \mu_{B_1}(y))$, $\alpha_2 = Min(\mu_{A_2}(x'), \mu_{B_2}(y))$,..., $\alpha_n = Min(\mu_{A_n}(x'), \mu_{B_n}(y))$.

Step 2: Evaluate the overall fuzzy inference $\mu_{B'}(y) = Max(\alpha_1, \alpha_2, \ldots, \alpha_n)$. After the fuzzy inference $\mu_{B'}(y)$ is evaluated, we compute the centroid of it by "center of gravity" method [21].

In the present control problem, x is error and y is displacement of the end-effector. The fuzzy rules constructed for the position control system are triggered appropriately depending on magnitude and sign of error signal and the selected rules on firing generate inferences, the union of which is the resulting control signal, representing

displacement of the end-effector. The fuzzy membership functions involving error are SMALL POSITIVE, etc. and angular displacement are SMALL NEGATIVE, etc. which are given in Fig. 2a, b and architecture of the proposed fuzzy controller is given in Fig. 2c. The list of fuzzy rules used for the generation of control signals is given below:

Rule 1: If error is SMALL POSITIVE then angular displacement is SMALL NEGATIVE.
Rule 2: If error is SMALL NEGATIVE then angular displacement is SMALL POSITIVE.
Rule 3: If error is NEAR ZERO then angular displacement is NEAR ZERO.
Rule 4: If error is LARGE NEGATIVE then angular displacement is LARGE POSITIVE.
Rule 5: If error is LARGE POSITIVE then angular displacement is LARGE NEGATIVE.

5 Experiments and Results

This section first describes the experimental protocol in a detailed way and represents the major outcomes of the experiment in subsequent stages. Key details of the experiment are highlighted below.

5.1 Subjects

Twelve people within a age group of 18–40 years (mean age 32) voluntarily participated in the study. None of them had any prior experience with BCI training. Out of the twelve volunteers, 6 were male, 6 were female, and 2 of them were differently abled (Sub11 and Sub12). The objective and procedure of experiment were made clear to the volunteers before conducting the experiment and a consent form stating their willingness to participate in the study was duly signed by them. The experiment was conducted in adherence to the Helsinki Declaration 1970 later revised in 2000 [22].

5.2 EEG System

EEG data were acquired from the volunteers using a 19 channel EEG amplifier device made by the company Nihon-Kohden. The EEG system has sampling rate 200 Hz and comes with built-in notch filter 50 Hz frequency. EEG electrodes were placed over the scalp by following the international 10–20 electrode placement convention

[23]. Out of the total 19 electrodes, we used six electrode positions (C_3, C_4, C_z over the motor cortex and P_3, P_4, Pz over the parietal lobe) to acquire the Motor Imagery brain signals. For the SSVEP and ErrP brain signals, we used $\{O_1, O2\}$ and $\{Fz, P_z\}$ electrode positions, respectively.

5.3 Training Session

We conducted the training session throughout the 15 d with a repetitions of 3 sessions in a day for each subject. Inter-session gap of 10 min was provided. Each session consists of 50 trials, resulting 150 trials for a subject in a day. Each trial contains the visual instruction to be followed by the participating subjects.

Visual instructions are presented before the subject through a robotic simulator. The robotic simulator virtually represents a robotic limb capable of producing clock/anti-clockwise movement around a specially designed fixed frame. The frame has markings of various positions over it along with the target position and LEDs are mounted near the frame against each positional markings. The LEDs flicker with a constant frequency but are different from each other.

A trial starts with a fixation cross that appears as a visual cue and asks the subject to remain alert for the upcoming visual cues. It stays on the screen for 2s duration. The next visual cue contains an instruction to perform either LEFT or RIGHT arm motor imagery for clockwise/anti-clockwise movement of the robotic limb. The next visual cue contains a scenario where the moving link commits an error by crossing the target location, hence the subject develops ErrP brain pattern by observing the error. The next scenario illustrates a condition where the end-effector of the moving link crossed the target position. Now, Subjects are instructed to focus their gaze on the flickering LED nearest to the present position of robot end-effector, focusing on the flickering source which generates an SSVEP signal modulated by the source frequency in the subjects' brain. Timing diagram of stimulus presentation is depicted in Fig. 3.

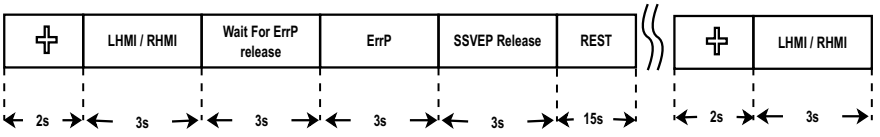

Fig. 3 Stimuli diagram of training session

5.4 Testing Session

The major difference between training session and testing session lies in the medium of operation. In contrast to the training session, which is conducted offline using a robotic simulator, the testing session is performed in real time with the physical robot. This session is more complex than training session as the subject participating in this session does not receive any visual instruction to perform the required mental task. Hence, the subjects need to plan the three steps of action (viz., link movement, target selection, and gazing on the nearest flickering source) themselves without any visual guidance.

A timing diagram presented in Fig. 4 shows the time taken by each module during real-time operation. During the real-time operation, we used a window of 1s duration to acquire the MI signal and SSVEP signal, whereas ErrP was acquired through the windows of 250 ms.

5.5 Results and Discussions

The results of the current experiment are presented in three stages. First, we provide a comparative analysis between the performance of the proposed feature extraction and classifier combination and other widely used methods in BCI literature. The performance is evaluated by averaging the performance of all the subjects over all the sessions during the testing phase. In the second stage, we provide performance analysis of all the subjects that participated in the testing session, and the performance of the proposed fuzzy controller is presented in the third stage.

Performance of the brain signal detection methods is evaluated on the basis of four metrics—Classification Accuracy (CA), True Positive Rate (TPR), False Positive Rate (FPR), and Cohen's kappa index (κ) as used in [15].

Performance of MI detection is presented in the first phase of Table 1. Along with the proposed Feature Extraction and Classifier combination (CSP + RBF SVM), we considered six other combinations to compare the performance. It is evident from the table that the proposed feature extraction+classifier combination worked best in our case yielding an average accuracy of 91.31% with average TPR, FPR, and kappa of 0.89, 0.04, and 0.84, respectively.

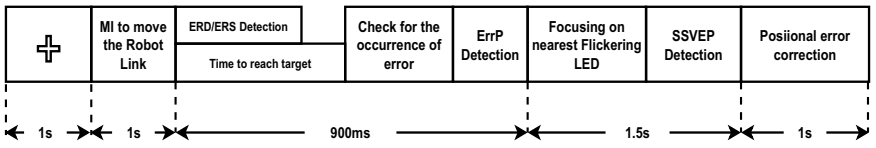

Fig. 4 Timing diagram of testing session

Table 1 Comparative study of different ERP detection methods

Brain pattern detection	Feature extraction + classifier	Performance metrics			
		CA (%)	TPR	FPR	kappa
MI detection	CSP+KSVM-RBF	91.31	0.89	0.04	0.84
	CSP+LSVM	90.11	0.89	0.05	0.83
	CSP+QDA	87.19	0.85	0.06	0.79
	DWT+KSVM-RBF	84.45	0.83	0.07	0.84
	DWT+QDA	88.56	0.89	0.05	0.80
	Hjorth+KSVM-RBF	82.38	0.81	0.09	0.75
	Hjorth+QDA	80.62	0.80	0.09	0.72
ErrP classifier	AAR+LSVM	92.71	0.91	0.04	0.82
	AAR+LDA	90.18	0.85	0.06	0.80
	Temporal Feature+ANN	83.13	0.82	0.07	0.76
	Temporal Feature+LDA	80.52	0.79	0.08	0.74
	SWLDA	91.23	0.90	0.04	0.81
SSVEP classifier	PSD(Welch)+Threshold	92.89	0.92	0.04	0.86
	PSD(Welch)+LSVM	93.80	0.93	0.03	0.85
	FFT	88.81	0.87	0.05	0.78
	CCA	94.96	0.94	0.02	0.88

CSP = Common Spatial Pattern
KSVM-RBF = Kernelized Support Vector Machine with Radial basis function kernel
LSVM = Linear Support Vector machine, DWT = Discrete Wavelet Transform
QDA = Quadratic Discriminant Analysis, LDA = Linear Discriminant analysis
ANN = Artificial Neural Network, CCA = Canonical Correlation Analysis

ErrP detection and SSVEP detection performances are compared with other relevant methods and results are presented in the second and third phases of Table 1. It is observed that average ErrP detection accuracy is achieved as high as 92% followed by the TPR, FPR, and kappa of 0.91, 0.04, and 0.82. Clearly, the present ErrP detection scheme outperforms the other methods by a significant margin.

We see a similar result in SSVEP performance, where the present SSVEP detection method achieves a moderately high detection accuracy of 93% with the TPR=0.92, FPR=0.04, and kappa=0.86. Although CCA here performs a little better than our proposed detection method, still we choose the proposed method for the major advantage of being computationally very inexpensive, hence most suitable for real-time operation.

Performances of all the subjects participated in the experiment are given in Tables 2, ,3, and 4. Each participant is evaluated through four metrics (CA, TPR, FPR, and kappa(κ)) described earlier. Average classification time taken by the clas-

Table 2 Subjectwise motor imagery detection result

Subject	Performance metrics (MI Detection)				
	CA% ± std	TPR	FPR	Kappa(κ)	Time(s)
Sub1	92.82±2.39	0.92	0.03	0.86	0.602
Sub2	93.96±1.82	0.92	0.03	0.91	0.549
Sub3	94.39±1.06	0.93	0.02	0.92	0.553
Sub4	89.81±2.21	0.86	0.03	0.81	0.608
Sub5	87.84±1.89	0.86	0.06	0.84	0.574
Sub6	94.49±1.84	0.92	0.04	0.89	0.579
Sub7	92.16±1.95	0.91	0.03	0.81	0.601
Sub8	91.87±1.26	0.89	0.04	0.83	0.583
Sub9	94.23±1.93	0.93	0.03	0.81	0.559
Sub10	93.12±1.28	0.93	0.05	0.84	0.552
Sub11	86.82±4.28	0.87	0.08	0.78	0.548
Sub12	84.23±3.73	0.85	0.07	0.76	0.571

Table 3 Subjectwise ErrP detection result

Subject	Performance metrics (ErrP detection)				
	CA% $\pm std$	TPR	FPR	Kappa(κ)	Time(s)
Sub1	94.81± 1.05	0.93	0.03	0.82	0.109
Sub2	94.52±1.01	0.94	0.04	0.90	0.113
Sub3	91.86±2.09	0.90	0.03	0.79	0.108
Sub4	93.47±0.98	0.92	0.04	0.81	0.121
Sub5	94.31±0.77	0.95	0.04	0.78	0.111
Sub6	93.28±1.46	0.92	0.03	0.93	0.107
Sub7	90.63±2.58	0.91	0.03	0.81	0.118
Sub8	89.86±2.81	0.88	0.03	0.85	0.105
Sub9	92.19±1.63	0.90	0.02	0.86	0.118
Sub10	90.25±2.28	0.90	0.06	0.78	0.108
Sub11	89.11±3.13	0.90	0.06	0.79	0.113
Sub12	86.28±2.08	0.85	0.05	0.72	0.110

sifier during the testing time is also reported in the above tables. Table 2 reveals that the highest detection accuracy of MI brain pattern is achieved for the sixth subject (CA=94.49%) while the third subject shows the highest kappa value of 0.92 indicating highest reliability. As revealed from Tables 3 and 4, the other two brain patterns, ErrP and SSVEP, were detected with maximum accuracy of 94.81% and 95.27%, respectively. The highest ErrP accuracy is observed with the first subject while the fifth subject shows the highest SSVEP accuracy. For the above two categories of signal, the highest kappa values are achieved as 0.93 and 0.92.

Table 4 Subjectwise SSVEP detection result

Subject	Performance metrics(SSVEP detection)				
	CA% ± std	TPR	FPR	Kappa(κ)	Time(s)
Sub1	93.88±0.89	0.92	0.02	0.91	0.091
Sub2	91.49±0.96	0.92	0.03	0.88	0.082
Sub3	91.90±0.93	0.90	0.04	0.82	0.095
Sub4	95.06±0.18	0.95	0.03	0.91	0.090
Sub5	95.27±0.27	0.94	0.02	0.92	0.086
Sub6	89.26±2.65	0.90	0.03	0.86	0.097
Sub7	92.43±1.03	0.91	0.03	0.87	0.092
Sub8	90.79±1.88	0.89	0.05	0.82	0.089
Sub9	93.72±0.98	0.94	0.05	0.81	0.103
Sub10	90.93±2.15	0.90	0.05	0.81	0.098
Sub11	85.89±5.05	0.84	0.08	0.72	0.089
Sub12	88.21±4.29	0.89	0.05	0.80	0.085

5.6 Comparison of System Performance

The overall position control performance of the system is evaluated using few popular metrics taken from control system literature. The metrics are success rate, steady-state error (SS error), peak overshoot, and settling time [14, 15].

Overall performance of the system is presented in Table 5. Results are averaged over all the subjects over all the testing sessions. Performance result is compared with five other relevant strategies. First the result is compared with the open-loop control strategy solely based on Motor Imagery [24]. Success rate obtained in this case found to be (76.2%). Next, the proposed method is compared with four hybrid BCI control strategies, where researchers, instead of relying on a single brain pattern, used multiple brain signals to design a robust interface for mentally controlling a robot arm. We considered four different control strategies that used four different combinations of brain signals (MI+SSVEP [25], MI+P300 [26], MI+ErrP [13], and MI+SSVEP+P300 [15]). Comparison results are obtained by implementing the control strategies in our own BCI setup.

It is evident from Table 5 that our proposed method achieves highest success rate (92.1%) among all the control strategies. It also ensured the lowest settling time (6s), steady-state error (0.15%), and peak overshoot (4.1%) among strategies under comparison. Although the present scheme shows improvement over all the fields considered in Table 5, the major improvement is considered to be the drastic reduction of settling time with simultaneous reduction of steady-state error and peak overshoot. Hence, the proposed fuzzy BCI controller outperforms the rest of the control strategies by a significant margin.

Table 5 Relative performance analysis

Strategies	Performance metrics			
	Success	SS	Peak	Settling
	Rate	Error(%)	Overshoot(%)	Time(s)
MI [24]	76.2	6.22	6.2	18
MI+SSVEP [25]	88.5	6.09	5.9	15
MI+P300 [26]	84.3	3.21	4.5	13
MI+ErrP [13]	85.8	2.1	4.9	16
MI+P300+SSVEP [15]	90.2	0.31	4.2	20
Proposed method	92.1	0.15	4.1	6

6 Conclusion

This paper claims to have utilized mentally generated sign and magnitude of positional error for automatic control of artificial robotic limb. The principles and realization of the above idea being novel in the realm of BCI are expected to open up new direction of control strategies, parallel to traditional controllers, as both the (approximate) magnitude and sign of positional error are known beforehand. Because of approximate estimation of positional errors, the logic of fuzzy sets has been incorporated that could handle the approximations and yields good control accuracy with small peak overshoot below 4.1% and settling time around 6 s.

References

1. Ha J, Kim L (2021) A brain-computer interface-based meal-assist robot control system. In: 2021 9th international winter conference on brain- computer interface (BCI). IEEE. 2021, pp 1–3
2. Ha J et al (2021) A hybrid brain-computer interface for real-life meal-assist robot control. Sensors 21(13):4578
3. Pfurtscheller G et al (2003) Graz-BCI: state of the art and clinical applications. IEEE Trans Neural Syst Rehabil Eng 11(2):1–4
4. Pfurtscheller G et al (2000) Current trends in Graz brain-computer interface (BCI) research. IEEE Trans Rehabil Eng 8(2):216–219
5. Liu Y et al (2018) Brain-robot interface-based navigation control of a mobile robot in corridor environments. IEEE Trans Syst Man Cybern: Syst 50(8):3047–3058
6. Tonin L, Bauer FC, Millán JDR (2019) The role of the control framework for continuous teleoperation of a brain-machine interface-driven mobile robot. IEEE Trans Robot 36(1):78–91
7. Chen X et al (2022) Clinical validation of BCI-controlled wheelchairs in subjects with severe spinal cord injury. IEEE Trans Neural Syst Rehabilitation Eng 30:579–589
8. Chen X et al (2019) Combination of high-frequency SSVEP-based BCI and computer vision for controlling a robotic arm. J Neural Eng 16(2):026012

9. Casey A et al (2021) BCI controlled robotic arm as assistance to the rehabilitation of neurologically disabled patients. Disabil Rehabil: Assist Technol 16(5):525–537
10. Vilela M, Hochberg LR (2020) Applications of brain-computer interfaces to the control of robotic and prosthetic arms. Handb Clin Neurol 168:87–99
11. Wang X et al (2022) Implicit robot control using error-related potential-based brain-computer interface. IEEE Trans Cogn Dev Syst
12. Iretiayo A et al (2020) Accelerated robot learning via human brain signals. In: IEEE international conference on robotics and automation (ICRA). IEEE, pp 3799–3805
13. Bhattacharyya S, Konar A, Tibarewala DN (2017) Motor imagery and error related potential induced position control of a robotic arm. IEEE/CAA J Autom Sin 4(4):639–650
14. Nagrath IJ, Gopal M (2007) Control systems engineering. In: New age international publishers, pp 193–268. ISBN: 81-224-2008-7
15. Rakshit A, Konar A, Nagar AK (2020) A hybrid brain-computer interface for closed-loop position control of a robot arm. In: IEEE/CAA J Autom Sin 7(5):1344–1360
16. Starczewski JT (2012) Advanced concepts in fuzzy logic and systems with membership uncertainty, Vol. 284. Springer, Berlin
17. Zimmermann H-J (2011) Fuzzy set theory-and its applications. Springer Science & Business Media
18. Lotte F, Guan C (2010) Spatially regularized common spatial patterns for EEG classification. In: 2010 20th international conference on pattern recognition. IEEE. 2010, pp 3712–3715
19. Bousseta R et al (2016) EEG efficient classification of imagined hand movement using RBF kernel SVM. In: 2016 11th international conference on intelligent systems: theories and applications (SITA). IEEE, pp 1–6
20. Carvalho SN et al (2015) Comparative analysis of strategies for feature extraction and classification in SSVEP BCIs. Biomed Signal Process Control 21 :34–42
21. Konar A (2006) Computational intelligence: principles, techniques and applications. Springer Science & Business Media
22. General Assembly of the World Medical Association et al (2014) World medical association declaration of Helsinki: ethical principles for medical research involving human subjects. J Am Coll Dent 81(3):14–18
23. Homan RW, Herman J, Purdy P (1987) Cerebral location of international 10–20 system electrode placement. Electroencephalogr Clin Neurophysiol 66(4):376–382
24. Bousseta R et al (2018) EEG based brain computer interface for controlling a robot arm movement through thought. Irbm 39(2):129–135
25. Yan N et al (2019) Quadcopter control system using a hybrid BCI based on off- line optimization and enhanced human-machine interaction. IEEE Access 8:1160–1172
26. Yu Y et al (2017) Self-paced operation of a wheelchair based on a hybrid brain-computer interface combining motor imagery and P300 potential. IEEE Trans Neural Syst Rehabil Eng 25(12):2516–2526